How to Cite: Zhortarova, A.A., Kubíček, V., Ibrayev, M.K., Panshina, S.Y., Pustolaikina, I.A., & Seidakhmetova, R.B. (2026) Cobalt(II) and Silver(I) Complexes with 2-Amino-4-Thiazolinone: Synthesis, Structural Characterization, and Antibacterial Potential. *Eurasian Journal of Chemistry.* https://doi.org/10.31489/2959-0663/4-26-4

Article

Received: 22 August 2026 | Revised: 30 October 2026|
Accepted: 3 November 2026 | Published online: 6 November 2026

UDC 544.42+519.242.7

https://doi.org/10.31489/2959-0663/4-26-4

Aigul A. Zhortarova[1], Vojtěch Kubíček[2], Marat K. Ibrayev[1], Svetlana Y. Panshina*[1], Irina A. Pustolaikina[1], Roza B. Seidakhmetova[3]

[1]*Chemistry Faculty, Buketov Karaganda National Research University, Karaganda, Kazakhstan*
[2]*Inorganic Chemistry Department, Faculty of Science, Charles University, Prague, Czech Republic*
[3]*Karaganda Medical University, Karaganda, Kazakhstan*
*(*Corresponding author's e-mail: janim_svetatusik@mail.ru)*

Cobalt(II) and Silver(I) Complexes with 2-Amino-4-Thiazolinone: Synthesis, Structural Characterization, and Antibacterial Potential

Selective control of amino- (**L_1**) and imino- (**L_2**) tautomeric forms of 2-amino-4-thiazolinone was achieved via precise pH regulation (pH 11 and 6.5, respectively) during hydrochloride precursor neutralization, as confirmed by ^{1}H and ^{13}C NMR spectroscopy. Reaction of protonated ligand with cobalt(II) chloride and silver(I) nitrate yielded [**$Co(L_1)_2Cl_2$**] and [**$Ag(L_1)_3NO_3$**] complexes. X-ray diffraction, IR, and UV–Vis spectral analyses revealed a distorted tetrahedral geometry for [**$Co(L_1)_2Cl_2$**] with monodentate endocyclic nitrogen coordination. In contrast, [**$Ag(L_1)_3NO_3$**] adopted an irregular coordination environment via endocyclic nitrogen and carbonyl oxygen atoms, assembling into chains. *In vitro* antimicrobial assays against Gram-positive (*S. aureus*, *B. subtilis*), Gram-negative (*E. coli*, *P. aeruginosa*) bacteria, and *Candida albicans* demonstrated a clear structure–activity relationship: free **L_1** < [**$Co(L_1)_2Cl_2$**] < [**$Ag(L_1)_3NO_3$**]. Uncoordinated **L_1** showed low-to-moderate activity (MIC = 64–128 μg/mL), silver complexation significantly enhanced potency, displaying broad-spectrum efficacy (MIC = 4–8 μg/mL) comparable to reference drugs. Molecular docking simulations against key microbial targets (DNA gyrase, penicillin-binding proteins, and CYP51) corroborated experimental findings, revealing the strongest binding affinity for [**$Ag(L_1)_3NO_3$**] (up to –8.8 kcal/mol against *S. aureus* DNA gyrase) stabilized by extensive hydrogen bonding, electrostatic, and hydrophobic interactions. These results highlight [**$Ag(L_1)_3NO_3$**] as a promising lead candidate for novel antimicrobial agents.

Keywords: 2-amino-4-thiazolinone, cobalt(II) complex, silver(I) complex, crystal structure, antimicrobial activity, tautomerism, DNA gyrase, molecular docking.

Introduction

Thiazolidin-4-one derivatives represent a crucial heterocyclic system, acting as a key pharmacophore and a privileged scaffold in medicinal chemistry. Due to the presence of the pharmacologically significant N–C–S fragment combined with a carbonyl group, these compounds possess immense therapeutic potential [1–3]. Systematic studies [1–6] in recent years have demonstrated a wide range of their biological activities, including antioxidant, anticancer, anti-inflammatory, analgesic, anticonvulsant, antiparasitic, and antiviral properties [6–8]. A special place among them is occupied by 2-amino-1,3-thiazol-4(5H)-one (2-amino-4-thiazolinone), a five-membered heterocyclic fragment containing sulfur and nitrogen donor atoms [9, 10]. This determines both its high reactivity and a pronounced tendency to coordinate with various metals [11, 12].

The biological activity of 2-aminothiazole derivatives has been actively studied over recent decades, primarily in the context of searching for novel, highly effective antibacterial and antimicrobial agents [13–

© 2026 The Authors. This is an open access article under the CC BY-NC-ND license (http://creativecommons.org/licenses/by-nc-nd/4.0/)

15]. The characteristic mechanism of their action is based on the ability of the thiazole core to participate in intermolecular interactions with biomolecular targets, as well as on the opportunities for targeted structural modification to optimize pharmacodynamic properties. Classical synthetic approaches to constructing the 2-amino-4-thiazolinone core are most frequently based on the cyclization methods of thiourea and thioamide derivatives [16–18].

Heterocycles containing N- and S-donor atoms are widely demanded as ligands for the design of transition metal complexes with unique catalytic and biologically relevant properties [19]. The literature describes numerous coordination compounds of azole derivatives with first-row transition metals (such as Cu(II), Ni(II), and Co(II)) [11, 12, 19–25]. In most cases, coordination with a metal leads to a significant change in the electron density of the ligand, as well as alterations in its symmetry and spatial configuration. This directly affects the nature of the complex's interaction with biomolecules, resulting in a substantial increase in biological activity compared to free organic molecules [24, 25].

The ligand 2-amino-4-thiazolinone exhibits ambidentate properties, as it contains three potential donor centers: a "hard" nitrogen atom (both in the thiazole ring and the amino group), a "soft" sulfur atom, and a carbonyl oxygen atom.

According to Pearson's Hard and Soft Acids and Bases (HSAB) principle [26, 27], metal ions can be classified by their coordination preferences. The silver(I) ion (Ag^+), possessing a stable d^{10} electronic configuration, belongs to the class of 'soft' acids and exhibits a high affinity toward 'soft' donor sites, such as the sulfur atom of the thiazole ring, frequently resulting in linear or coordination-unsaturated structures with strong Ag–S bonds [28]. Conversely, the cobalt(II) ion (Co^{2+}) is a 'borderline' acid with a d^7 configuration, which enables effective coordination with both 'borderline' nitrogen and 'hard' oxygen donor atoms, typically forming stable octahedral or tetrahedral chelate complexes [28, 29].

Thus, the choice of these two metals allows for the investigation of how the nature of the cation ("soft" versus "borderline") influences the competition between the donor centers (N, S, or O) of the same ligand, and how the crystal structure changes in a directed manner (a polymeric chain for silver versus a discrete mononuclear complex for cobalt)

Modern drug design necessitates a mandatory combination of experimental methods with computational approaches (*in silico*) [30]. Conducting virtual screening and molecular docking [4] allows for the identification of the most probable enzymatic targets among bacterial proteins. Studying the spatial and energetic complementarity of synthesized transition metal complexes within the active sites of these proteins opens the way to understanding the molecular mechanisms of their antibacterial action.

The aim of this study was the controlled synthesis of the amino ($\mathbf{L_1}$) and imino ($\mathbf{L_2}$) tautomeric forms of 2-amino-4-thiazolinone (Figure 1), via precise pH control during the neutralization of its hydrochloride precursor, the investigation of their coordination behavior toward cobalt(II) and silver(I) ions (Figure 2), and the definitive structural elucidation of the resulting complexes, [$\mathbf{Co(L_1)_2Cl_2}$] and [$\mathbf{Ag(L_1)_3NO_3}$], using IR, electronic spectroscopy, and X-ray diffraction (XRD) analysis. An additional objective of the study was a comprehensive *in vitro* evaluation of the antimicrobial and antifungal potential of the synthesized compounds, combined with preliminary *in silico* prediction of biological activity and molecular docking to substantiate the "structure–activity" relationship (SAR).

Experimental

Materials and Methods

Commercially available reagents: thiourea, ethyl chloroacetate, cobalt(II) chloride hexahydrate, and silver nitrate were used without further purification unless otherwise stated; solvents were dried by standard procedures. Melting and boiling points were determined in open capillaries using a Buchi M560 device. The IR spectra were obtained using a FSM 1201 FT-IR spectrophotometer in a KBr tablet (neat) in the frequency range: 4000–400 cm^{-1}, using KBr pellets (ν / cm^{-1}). The progress of reactions was accomplished by thin-layer chromatography (TLC) analysis on coated silica plates (Silufol, UV-254 TLC, aluminum sheets) and plates were visualized with UV light (at 254 nm).The ^1H and ^{13}C NMR spectra were recorded on a Bruker Avance III spectrometer (400 MHz for ^1H NMR, 100 MHz for ^{13}C NMR) using DMSO-d_6 solvent with tetramethylsilane (TMS) as internal standard. Chemical shifts (δ) are given in ppm, and the coupling constants (*J*) are given in Hz, respectively. X-ray diffraction data for single crystals were collected using a Bruker APEX diffractometer with a Mo Kα radiation source (λ = 0.71073 Å). Crystal structures were solved and refined using the SHELXT/SHELXL program package (Sheldrick, G.M., Acta Cryst. 2015). Visualization and analysis of crystal structures were performed with Mercury software (CCDC, Cambridge, UK), which

enables three-dimensional structural representation, analysis of non-covalent interactions, and generation of publication-quality figures. Absorption spectra were recorded on a Shimadzu UV-1800 spectrophotometer in Ethanol. The metal content (cobalt and silver) was determined using an AA-140 atomic absorption spectrometer with a flame atomizer (air-acetylene). The analytical parameters were as follows: for Co, λ = 240.7 nm, slit width 0.2 nm, and lamp current 7 mA (linear range: 0.05–15 μg/mL); for Ag, λ = 328.1 nm, slit width 0.5 nm, and lamp current 4 mA (linear range: 0.02–10 μg/mL).

Synthetic Procedures

2-Amino-4-thiazolinone hydrochloride (L). 100 mL of 95% ethanol and 38 g (0.5 mol) of thiocarbamide were placed in a 500 mL single-neck flask equipped with a reflux condenser. Then, 54 mL (0.5 mol) of ethyl chloroacetate was added. The mixture was refluxed for 3 hours, during which the formation of a white crystalline precipitate was observed. The resulting product, in the form of hydrochloride, was filtered off and washed with ethanol. Yield: 66.9 g of 2-amino-4-thiazolinone hydrochloride **L** (88%).

2-Amino-4-thiazolinone (L_1). 2-Amino-4-thiazolinone hydrochloride **L** (66.9 g) was dissolved in 100 mL of a 25% aqueous ammonia solution to obtain white crystalline reprecipitated 2-amino-4-thiazolinone $\mathbf{L_1}$ with a yield of 44.9 g (83%). M.p. (decomp.): 255–258 °C. ^{1}H NMR spectrum, δ, ppm: 8.95 (br s, 1H, NH_2), 8.76 (br s, 1H, NH_2), 3.89 (s, 2H, CH_2) (Figure S1). ^{13}C NMR spectrum, δ, ppm: 188.27 (C–NH_2), 183.34 (C=O), 40.32 (CH_2) (Figure S2). IR spectrum, ν, cm^{-1}: 3377, 3398 (NH_2), 2986 (CH), 1651 (C=O), 1524 (C=N), 706 (C–S) (Figure S3). UV–vis (ethanol) λ_{max}: 220, 250.5 nm (Figure 5).

2-Imino-4-thiazolidinone (L_2). 2-Amino-4-thiazolinone hydrochloride **L** (66.9 g) was dissolved in 500 mL of hot water, and 60 g of sodium acetate was added to the boiling solution. The mixture was heated to boiling and then cooled; the transparent solution was left in a cold place for 24 hours. The formed white crystals were filtered off and air-dried. The resulting 2-imino-4-thiazolidinone $\mathbf{L_2}$ was obtained in an amount of 42.7 g (79%); it is insoluble in organic solvents and soluble in water. M.p. (decomp.): 205–208 °C. ^{1}H NMR spectrum, δ, ppm: 10.98 (br s, 1H, NH), 6.58 (br s, 1H, NH), 4.10 (s, 2H, CH_2) (Figure S4). ^{13}C NMR spectrum, δ, ppm: 178.65 (C=O), 177.62 (C=NH), 37.23 (CH_2) (Figure S5). IR spectrum, ν, cm^{-1}: 3380 (NH), 2987 (CH), 1678 (C=O), 1540 (C=N), 708 (C–S).

Complex $[Co(L_1)_2Cl_2]$. 2-Amino-4-thiazolinone hydrochloride $\mathbf{L_1H}$ (0.256 g, 2.0 mmol) was dissolved in acetonitrile (20 mL). Cobalt(II) chloride hexahydrate (0.238 g, 1.0 mmol) was added, and the mixture was refluxed under stirring for 24 h (pH = 5.5). After slow cooling, blue crystals were obtained, filtered, washed with cold acetonitrile, and dried in air. Yield is (0.49 g) 68%. M.p. (decomp.): 260 °C. ^{1}H NMR spectrum, δ, ppm: 9.20 (br s,1H, NH_2), 7.77 – 7.23 (m, 1H, NH_2), 4.02 (s, 2H, CH_2) (Figure S6). IR spectrum, ν, cm^{-1}: 3402 (NH_2), 3071 (CH), 1608 (C=O), 1585 (C=N), 771 (C–S), 478, 416 (Co–N) (Figure S7). Atomic absorption analysis: Calcd (%) for $C_6H_8Cl_2CoN_4O_2S_2$: Co, 16.27. Found (%): Co, 16.25. UV–vis (ethanol) λ_{max}: 227.5, 264 nm (Figure 5).

Complex$[Ag(L_1)_3NO_3]$. 2-Amino-4-thiazolinone hydrochloride $\mathbf{L_1H}$ (0.384 g, 3.0 mmol) was dissolved in acetonitrile (20 mL) under exclusion of light. Silver nitrate (0.170 g, 1.0 mmol) was added, and the reaction mixture was refluxed for 12 h. After slow evaporation in the dark, green crystals were obtained, filtered, washed with acetonitrile, and dried. Yield is (0.32 g) 61%. M.p. (decomp.): 265 °C. ^{1}H NMR spectrum, δ, ppm: δ 8.89 (br s, 1H, NH_2), 7.31 – 7.05 (m, 1H, NH_2), 3.71 (s, 2H, CH_2) (Figure S8). IR spectrum, ν, cm^{-1}: 3414 (NH_2), 3067 (CH), 1639 (C=O), 1554 (C=N), 1388–1304 (NO_3^-), 474 and 574 (Ag–L). (Figure S9). Atomic absorption analysis: Calcd (%) for $C_9H_{12}AgN_7O_6S_3$: Ag, 20.81. Found (%): Ag, 20.95. UV–vis (ethanol) λ_{max}: 209, 264 nm (Figure 5).

Antimicrobial Activity

Antimicrobial activity of synthesized compounds – cobalt(II) complex $\mathbf{[Co(L_1)_2Cl_2]}$ and silver(I) complex $\mathbf{[Ag(L_1)_3NO_3]}$ – was evaluated against two Gram-positive bacteria (Staphylococcus aureus ATCC 25923 and Bacillus subtilis ATCC 6633), two Gram-negative bacteria (Escherichia coli ATCC 25922 and Pseudomonas aeruginosa ATCC 27853), and pathogenic fungus Candida albicans ATCC 10231. Screening was carried out by both disk diffusion method on Müller–Hinton agar. Sterile paper disks impregnated with 20 μL of compound solution (1 mg/mL) were applied to inoculated agar plates standardized to 0.5 McFarland turbidity and broth microdilution method for determination of minimum inhibitory concentration (MIC), in accordance with CLSI guidelines [31, 32]. Ampicillin, ciprofloxacin, and fluconazole were used as reference standards for Gram-positive bacteria, Gram-negative bacteria, and fungi, respectively. All experiments were performed in triplicate, and results are expressed as mean ± standard deviation.

Docking Studies

Molecular docking studies were performed in accordance with the protocol described in [33] using AutoDock Vina version 1.1.2 [34]. For coordination complexes containing Co^{2+} and Ag^{+} ions, metal center parameters were explicitly assigned prior to docking. Atomic partial charges for the metal centers and coordinated ligand environments were derived using DFT calculations [35] (B3LYP 6-311++G(d,p) level of theory for light atoms and LanL2DZ pseudopotential for Co/Ag) via Mulliken population analysis with the help Gaussian-16 [36]. Custom AutoDock force field parameters for cobalt and silver ions (including non-bonded Lennard-Jones parameters ε and σ, ionic radii, and coordination geometries) were integrated into the force field files following the AutoDock metal parameterization protocols. Target protein 3D crystal structures were retrieved from the RCSB Protein Data Bank: DNA gyrase from *E. coli* / *P. aeruginosa* (PDB ID: 6RKS [37]), DNA gyrase from *S. aureus* (PDB ID: 2XCT [38]), penicillin-binding protein from *E. coli* (PDB ID: 2EXB [39]), penicillin-binding protein from *S. aureus* (PDB ID: 1VQQ), and CYP51 from *Candida albicans* (PDB ID: 4WMZ [40]).

Ligand structures were prepared and energy-minimized using Chem3D (ChemOffice package, PerkinElmer). A semi-flexible docking protocol was employed, wherein the receptors were kept rigid while full conformational flexibility was allowed for the ligands [41]. Active site grid coordinates were centered on the native ligand binding pockets as follows: $x = 158.511, y = 158.419, z = 127.835$ (6RKS); $x = -6.335, y = 40.298, z = 94.133$ (2XCT); $x = 93.031, y = 10.175, z = 45.264$ (2EXB); $x = -0.697, y = 34.862, z = 44.548$ (1VQQ); and $x = 9.522, y = 10.492, z = 17.031$ (4WMZ). The Lamarckian Genetic Algorithm (LGA [42]) implementation in AutoDock Vina was utilized to search the conformational space. Calculated binding affinities (kcal/mol) and non-covalent ligand–receptor interaction networks were evaluated using Discovery Studio Visualizer (Dassault Systèmes BIOVIA).

Results and Discussion

Chemistry

2-Amino-4-thiazolinone (**L₁**) and its tautomeric form, 2-imino-4-thiazolidinone (**L₂**) (Figure 1), as well as their classical isosteres – glitazone (1,3-thiazolidine-2,4-dione) and rhodanine (2-thioxo-1,3-thiazolidin-4-one), are of significant pharmacological interest [43-44]. In this work, the possibility of using 2-amino-4-thiazolinone (**L₁**) as a ligand has been investigated in its protonated form (**L₁H**), as well as in two tautomeric forms. It was previously shown by IR and NMR spectroscopy [9, 10] that 2-amino-4-thiazolinone (**L₁**) exists predominantly in the amino form (**L₁**) both in the crystalline state [45] and in solutions. Nevertheless, the structure of the imine form **L₂**, as well as the conditions for the tautomeric proton transfer in the molecule during the isolation process, are practically not discussed in the literature.

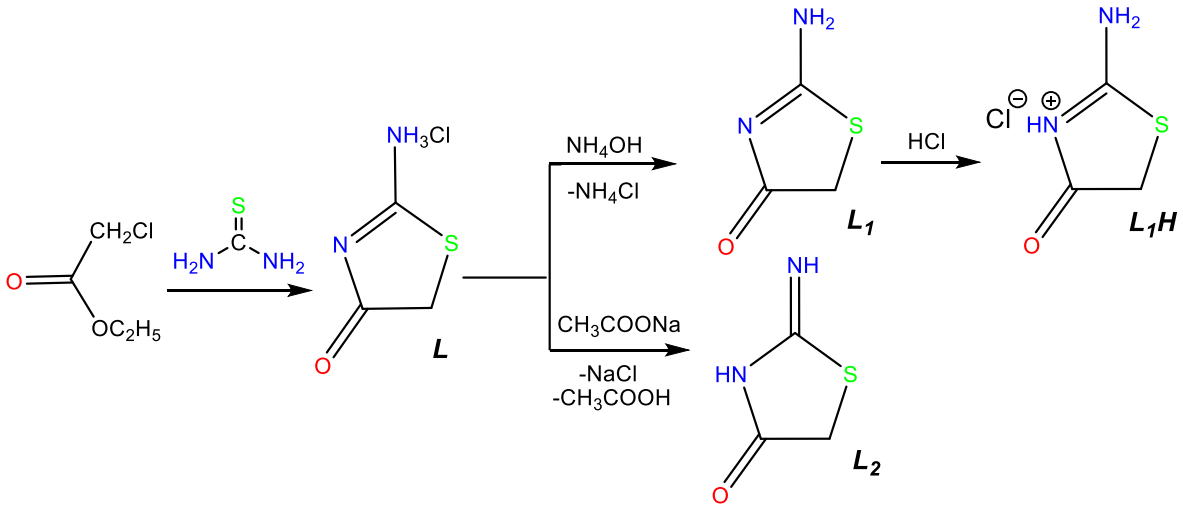


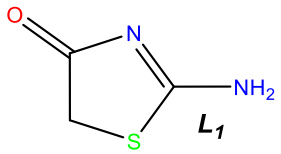
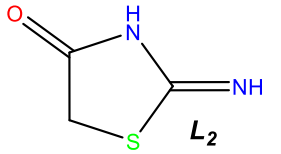
Figure 1. Synthesis of amino (**L₁**) and imino (**L₂**) tautomeric forms of 2-aminothiazol-4-one

We have demonstrated that the direction of the tautomeric shift (amino–imine form) can be controlled by varying the neutralization conditions of 2-amino-4-thiazolinone hydrochloride (**L**). It was found that in a strongly alkaline medium (pH = 11, aqueous ammonia), hydrochloride **L** converts predominantly into the

amino form **L₁**. Meanwhile, treatment of compound **L** with a sodium acetate solution (pH = 6.5) results in the formation of the imine structure **L₂** (Figure 1). The amino (**L₁**) and imino (**L₂**) forms of thiazolinone thus obtained were studied by NMR spectroscopy (Table 1).

Table 1

^{1}H and ^{13}C NMR spectra of amino (L₁) and imino (L₂) tautomeric forms of 2-aminothiazol-4-one

Compound	NMR spectra in DMSO-d_6, δ, ppm					
	^{1}H NMR spectrum			^{13}C NMR spectrum		
 **L₁**	NH_2	–	CH_2	C–NH_2	C=O	CH_2
	8.95 8.76	–	3.89	188.27	183.34	40.32
 **L₂**	NH	NH	CH_2	C=NH	C=O	CH_2
	10.98	6.58	4.10	177.62	178.65	37.23

The PMR spectroscopy data (Table 1) provide direct evidence of the tautomeric state. For the amino form (**L₁**), two signals are observed at 8.95 and 8.76 ppm, which is characteristic of the non-equivalent protons of the NH_2-group. The absence of signals in a downfield region (above 10 ppm) indicates that the endocyclic nitrogen is not protonated. For the imine form (**L₂**), the spectrum changes fundamentally, exhibiting two singlets at 10.98 and 6.58 ppm. This corresponds to two chemically distinct protons of the groups: =NH (exocyclic imine group) and –NH– (endocyclic nitrogen). The signal of the methylene CH_2 ring protons in **L₂** is shifted downfield (4.10 ppm versus 3.89 ppm for **L₁**), which is explained by the increased deshielding effect from the double bond system in the imine form.

The carbon chemical shifts provide insight into the change in the electronic density within the ring. For the amino form, the carbon signal of the C–NH_2 group is observed at 188.27 ppm, whereas for the imine form (C=NH), it shifts upfield to 177.62 ppm. A difference of more than 10 ppm serves as a marker for distinguishing between amino and imine thiazole derivatives. The signal of the carbonyl carbon (C=O) at 183.34 ppm in **L₁** shifts to 178.65 ppm in **L₂**, indicating a redistribution of conjugation within the molecule upon proton transfer to the endocyclic nitrogen. The chemical shift values of the methylene CH_2-group (40.32 ppm for **L₁** and 37.23 ppm for **L₂**) also correlate with the changes in hybridization and charge distribution within the heterocycle.

The registration of two separate, non-overlapping sets of resonance lines in the ^{1}H and ^{13}C NMR spectra of **L₁** and **L₂** in DMSO-d_6 (Table 1) – without cross-peaks or traces of the counterpart tautomer – indicates that the rate of the prototropic **L₁** ⇌ **L₂** tautomeric exchange is extremely low under these experimental conditions. In polar aprotic media such as DMSO-d_6, the high activation barrier for the 1,3-proton shift in the absence of protic catalysts prevents rapid equilibration. Thus, the selective isolation driven by pH adjustment during neutralization (pH 11 for **L₁** vs. pH 6.5 for **L₂**) yields kinetically stable tautomeric forms that maintain their structural integrity upon dissolution during the timeframe of the NMR analysis.

In transitioning from the study of free ligands to the synthesis of coordination compounds, it was found that the reactivities of tautomers **L₁** and **L₂** differ significantly. The protonated form of 2-amino-4-thiazolinone (**L₁H**) was chosen as the starting substrate for the preparation of silver and cobalt complexes. It was experimentally established that the use of neutral free forms **L₁** and **L₂** leads to a significantly lower yield of the target products or the formation of multiphase mixtures, indicating their lower activity in complexation processes under the selected conditions

The synthesis of silver and cobalt complexes was carried out in acetonitrile while varying the metal-to-ligand molar ratios (Figure 2). The reaction with cobalt(II) chloride hexahydrate at a 2:1 ratio leads to the formation of the **[Co(L₁)₂Cl₂]** complex, whereas the interaction with silver(I) nitrate (3:1) proceeds with ligand deprotonation to form the three-coordinate **[Ag(L₁)₃NO₃]** complex.

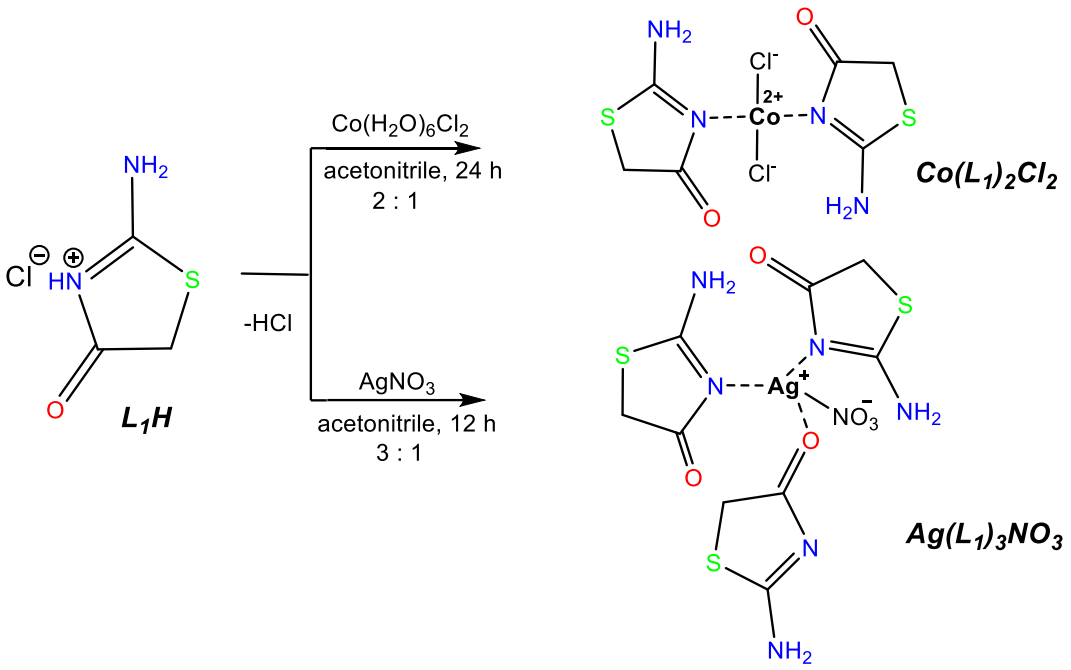


Figure 2. Synthesis of cobalt(II) and silver(I) complexes based on the protonated form of 2-amino-4-thiazolinone (**L_1H**)

The reaction of 2-amino-4-thiazolinone hydrochloride (**L_1H**) with cobalt (II) chloride confirmed its high complexing ability, yielding a stable, deep-blue crystalline product. Similarly, the interaction with silver (I) nitrate resulted in a green complex compound with a melting point of approximately 250°C. Such a high melting point indicates the significant thermal stability of the obtained silver complex. The formation of these solid crystalline products further demonstrates the successful coordination of Co^{2+} and Ag^{+} ions with the heterocyclic ligand.

The ^{1}H NMR spectra of the **$[Co(L_1)_2Cl_2]$** (Figure S6) and **$[Ag(L_1)_3NO_3]$** (Figure S8) complexes in DMSO-d_6 exhibit very similar profiles in the standard diamagnetic region (0–10 ppm), featuring characteristic broadening of the NH_2 proton resonances (δ = 9.20 ppm for Co(II) and δ = 8.89 ppm for Ag(I)). Since silver(I) is a diamagnetic d^{10} ion, the observed line broadening and spectral similarity across both complexes indicate a common solution-state dynamic behavior driven by solvent-assisted ligand exchange and equilibrium with the free ligand in a strongly coordinating solvent (DMSO-d_6) rather than a rigid coordination state or purely paramagnetic distortion.

X-ray Structural Analysis of Cobalt(II) and Silver(I) Complexes

Confirmation of the structures of the synthesized **$[Co(L_1)_2Cl_2]$** and **$[Ag(L_1)_3NO_3]$** complexes and determination of their geometry in the crystalline phase were achieved using single-crystal X-ray diffraction (XRD) analysis. Based on the obtained diffraction data, the crystal structures of both the starting 2-amino-4-thiazolinone hydrochloride (**L_1H**) and the corresponding cobalt(II) and silver(I) coordination compounds were solved and refined (Figure 3).

Structural analysis indicates that the ligand in the complexes exists exclusively in the amino-form, coordinating predominantly via the endocyclic nitrogen atom. The obtained XRD data are in complete agreement with the results of IR (Figure 4) and UV spectroscopy (Figure 5), as well as atomic absorption analysis, forming a coherent picture of the structure of the studied objects.

The deep-blue complex **$[Co(L_1)_2Cl_2]$**, bis(2-amino-4-thiazolinone)dichlorocobalt (II)**,** crystallises in the triclinic space group *P*1 (No. 2). The cobalt(II) center adopts a tetrahedral coordination geometry, formed by two chloride anions and two molecules of the ligand **L_1** coordinated via the endocyclic nitrogen atoms. The bond angles around the metal center deviate slightly from the ideal tetrahedral value (109.47°): the Cl–Co–Cl angle is 110.98°, the N–Co–N angle is 103.15°, and the C–Co–N angles range between 109.96 and 112.50°.

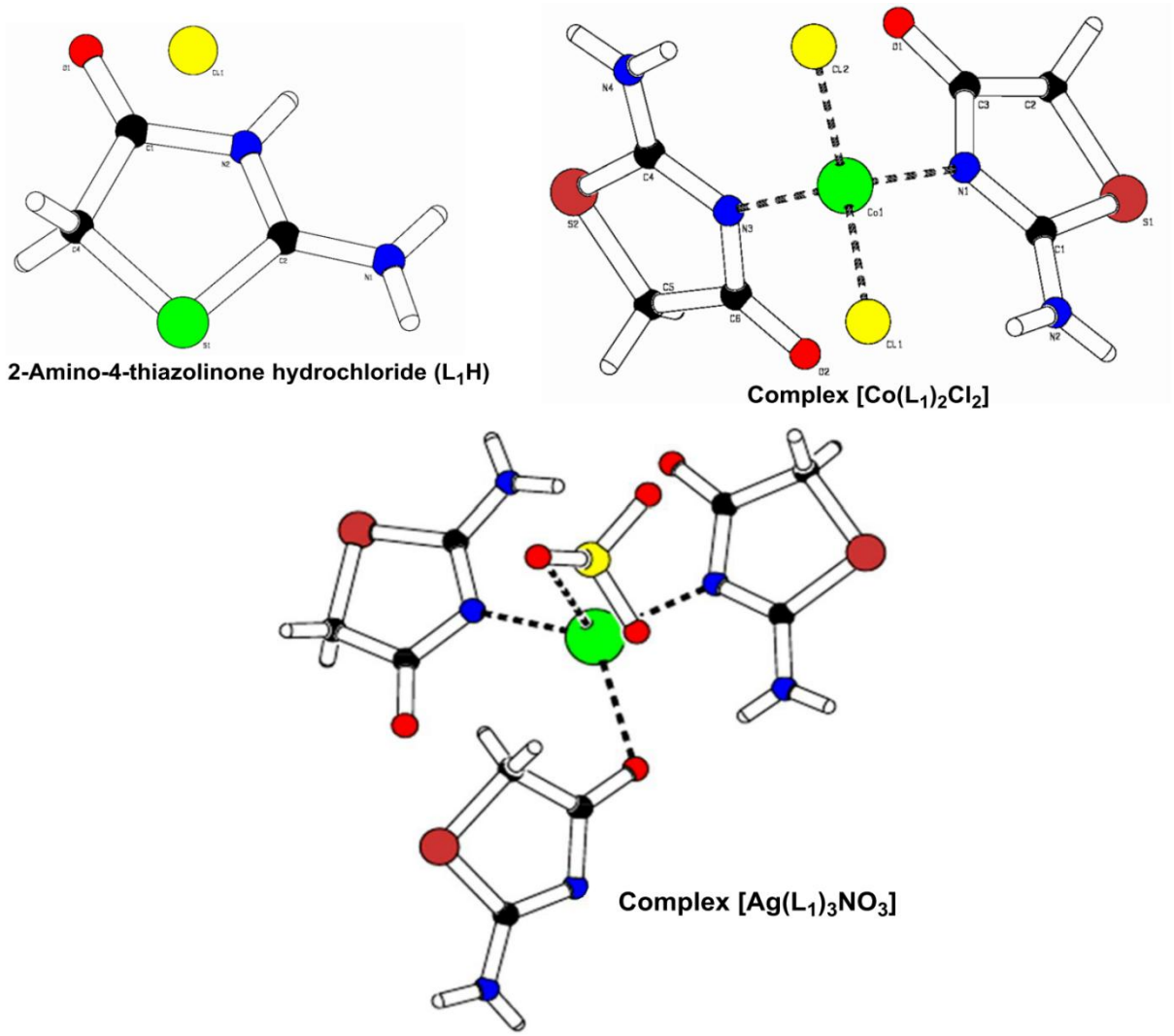


Figure 3. Molecular structures of 2-amino-4-thiazolinone hydrochloride (**L_1H**) and its complexes **$[Co(L_1)_2Cl_2]$** and **$[Ag(L_1)_3NO_3]$** according to single-crystal X-ray diffraction data

These values confirm a slightly distorted tetrahedral environment for the Co(II) ion. The carbonyl oxygen atoms and the nitrogen atoms of the amino groups remain uncoordinated. The geometry of the coordinated heterocyclic moieties is nearly identical to that observed in the "free" ligand **L_1H**. Specifically, atoms O_1 and N_1 (as well as O_2 and N_2) lie within the planes of the five-membered rings. The cobalt center (Co) is displaced from the mean planes of the ligand rings by only approximately 0.2 Å. The hydrogen-bonding network in the complex is relatively simple compared to that in the precursor salts. One hydrogen atom of each amino group forms an intramolecular H-bond with a chloride ligand (D … A distances of 3.266(2) and 3.261(3) Å). The second amino hydrogen atom participates in an intermolecular H-bond with the carbonyl oxygen atom (O_1) of a neighboring molecule (D … A distances of 2.834(4) and 2.882(3) Å). These intermolecular contacts unite the complex molecules into infinite chains, which are further stabilized in the crystal packing by weak π-π stacking interactions with interplanar distances of approximately 3.5 Å.

The green complex **$[Ag(L_1)_3NO_3]$,** tris(2-amino-4-thiazolinone)silver (I) nitrate, crystallizes in the monoclinic space group *P*21/*n* (No. 14) as plate-like crystals. The coordination environment of the central Ag(I) atom is irregular. The first coordination sphere involves the N_1 and N_2 nitrogen atoms of two independent 2-amino-4-thiazolinone rings, the carbonyl oxygen atom of an adjacent ligand **L_1** molecule (with a d(Ag–O) distance of 2.490(1) Å), and a NO_3^- anion coordinated via the O_1 atom with a (Ag–O_1) distance of 2.816(1) Å. Although this value exceeds the typical bond lengths for strong coordination (2.6–2.7 Å), the presence of the interaction is confirmed by the redistribution of electron density within the nitrate anion. The N–O_1 bond is elongated by approximately 0.03 Å relative to the average values of the other N–O bonds, indicating a noticeable polarization of the anion upon coordination to the metal. The geometry of the complex

is heavily distorted: the maximum valence angle is 143.32(5)° (N_1–Ag–N_2), while the minimum is 81.52(6)° (N_1–Ag–O).

At the same time, the silver atom maintains a planar environment relative to the ligands, deviating from the planes of their rings by only 0.12 Å. Such irregular geometry and the presence of "long" contacts with the anion are characteristic of Ag(I) ions with their flexible d^{10} shell, which promotes the formation of complex chains in the crystal due to bridging carbonyl groups.

The stability of the crystal packing of the complex is ensured by a complex network of intermolecular hydrogen bonds (Figure S10). The amino groups of the ligands form strong N–H…O (nitrate) hydrogen bonds with the oxygen atoms of the nitrate anion that are not involved in direct coordination to the silver atom. Intermolecular interactions are also observed between the NH_2-group of one complex and the carbonyl oxygen (C=O) of the ligand in an adjacent **L_1** molecule. These bonds contribute to the additional fixation of the anion in the crystal lattice and compensate for its weak coordination bond with the metal; they are of medium strength, with lengths ranging from 2.8 to 2.9 Å and angles of 160–170°.

The geometry of the ligand arrangement around the central Ag(I) atom favors the formation of weak intramolecular contacts, which stabilize the conformation of the "tris-chelate" environment despite significant distortions of the bond angles. Since metal coordination is accompanied by a redistribution of electron density within the ligand molecules, this must inevitably lead to a change in the force constants of the chemical bonds and, consequently, to a shift in the corresponding characteristic vibrational frequencies.

IR Spectroscopy of Cobalt(II) and Silver(I) Complexes

An effective method for confirming the complex nature of synthesized compounds is the joint analysis of their vibrational spectra alongside the spectrum of the initial organic substrate. The presented overlay of the IR spectra of **L_1** (2-amino-4-thiazolinone) and the synthesized complexes **$[Co(L_1)_2Cl_2]$** and **$[Ag(L_1)_3NO_3]$** (Figure 4) clearly illustrates the transformation of the spectral profile in the regions of the amino group stretching vibrations (3400–3100 cm^{-1}) and the heterocyclic fragment (1650–1500 cm^{-1}). These changes correlate with the proposed coordination mode and the alteration of the system's symmetry.

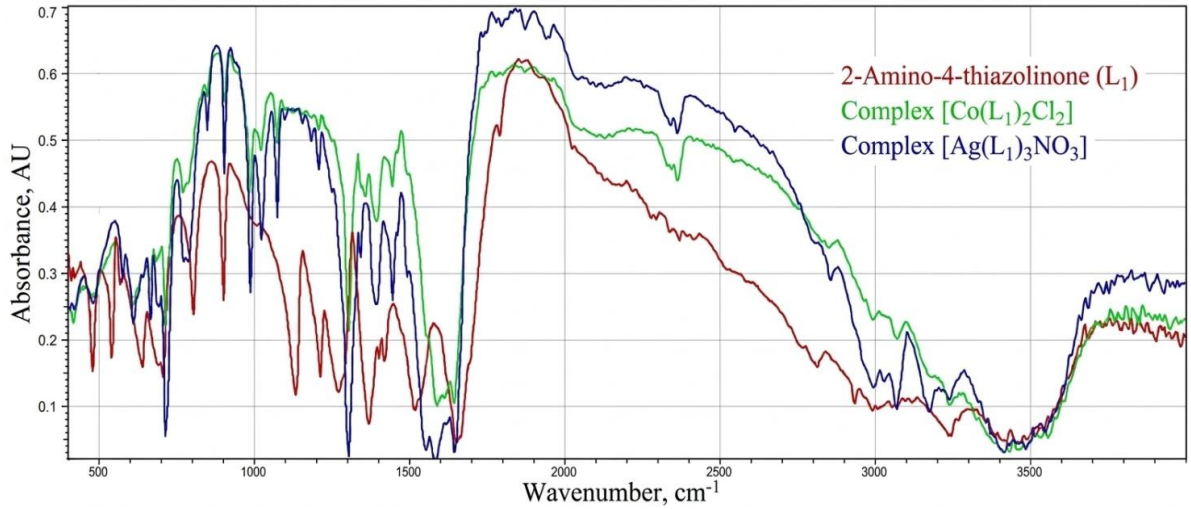


Figure 4. Comparison of the IR absorption spectra of the free ligand **L_1** (2-amino-4-thiazolinone) and the synthesized complexes **$[Co(L_1)_2Cl_2]$** and **$[Ag(L_1)_3NO_3]$**

In the spectrum of the free ligand **L_1** (Figures 4, S3), the following key characteristic bands are observed: the high-frequency peak at 3398 cm^{-1} corresponds to the ν(NH_2) stretching vibrations. The bands in the region of 2986–2804 cm^{-1} are assigned to the stretching vibrations of the ring CH and CH_2 groups. The intense band at 1651 cm^{-1} is responsible for the stretching vibrations of the double bond, ν(C=O). The band at 1524 cm^{-1} is characteristic of the conjugated N–C=N or C=C system. The peaks at 1369, 1207, and 1130 cm^{-1} are attributed to the skeletal vibrations of the ring and deformation vibrations of the CH_2-groups. The band at 706 cm^{-1} can be assigned to the stretching vibrations, ν(C–S), of the thiazoline ring.

A comparison of the IR spectrum of the cobalt complex **$[Co(L_1)_2Cl_2]$** with that of the free ligand **L_1** (Figures 4, S7) allows for a conclusion regarding the coordination mode, which is fully supported by the XRD data. In the spectrum of the complex, the ν(NH_2) band shifts to 3402 cm^{-1}, whereas the appearance of

new components in the 3236–3071 cm^{-1} region is attributed to alterations in the hydrogen-bonding system upon molecular packing in the crystal, given that the amino group, according to the XRD data, is not directly involved in coordination with the metal ion. The most significant changes occur in the absorption region of the heterocycle: the band at 1651 cm^{-1} shifts to the lower-frequency region (1608–1585 cm^{-1}), which is driven by the redistribution of electron density within the conjugated O=C–N=C ring system upon binding of the Co^{2+} ion to the endocyclic nitrogen atom. The shift of the ν(C–S) bands to the 771 and 600 cm^{-1} regions also points to the involvement of the heterocycle in complexation. Coordination via the endocyclic nitrogen atom is further confirmed by the emergence of new bands in the low-frequency region at 478 and 416 cm^{-1}, which are assigned to the metal–ligand ν(Co–N) stretching vibrations

The IR spectrum of the silver complex **[Ag(L₁)₃NO₃]** reflects a more complex coordination behavior (Figures 4, S9), which is driven by the presence of two types of chemically non-equivalent **L₁** ligands within the unit cell. The significant broadening and splitting of the bands in the 3414–3067 cm^{-1} region are attributed to a complex network of intermolecular contacts. In the region of the C=O and C=N stretching vibrations, the appearance of several well-defined peaks at 1639, 1581, and 1554 cm^{-1} is observed. This is in excellent agreement with the XRD data, which indicate a monodentate binding mode for all ligands, albeit via different donor centers: the band at 1639 cm^{-1} corresponds to the carbonyl group coordinated through the oxygen atom, ν(C=O → Ag), whereas the shift of the bands in the 1581–1554 cm^{-1} region is caused by the coordination of the other two ligand molecules via the endocyclic nitrogen atoms of the heterocycle. A characteristic feature of the spectrum of this complex is an intense, broad band in the 1388–1304 cm^{-1} region, signifying the presence of the nitrate anion (NO_3^-). The shift and splitting of the deformation vibrations in the 895–713 cm^{-1} region confirm that the nitrate group enters the inner coordination sphere of the silver ion, exhibiting a monodentate coordination mode. The bands of medium intensity at 574 and 474 cm^{-1} are assigned to the ν(Ag–O) and ν(Ag–N) stretching vibrations, respectively.

Thus, contrary to the initial assumption of chelate binding, the combined analysis of IR spectroscopy and XRD data rigorously proves the monodentate coordination mode of the ligand **L₁**: exclusively via the endocyclic nitrogen atom in the cobalt(II) complex, and a mixed (N- or O-donor) coordination type in the silver(I) complex. Additional information regarding the electronic state of the system and changes in the molecular energy levels upon complexation was obtained by electronic absorption spectroscopy.

Electronic Absorption Spectroscopy of Cobalt(II) and Silver(I) Complexes

A comparative analysis of the spectra of the free ligand **L₁** and its complexes with cobalt(II) and silver(I) allows monitoring the redistribution of electron density and evaluating the influence of the central ion on the π → π* and n → π* transitions of the organic **L₁** molecule [46].

Figure 5 presents the electronic absorption spectra (UV-Vis) of the free ligand **L₁** (2-amino-4-thiazolinone) and the synthesized coordination compounds of 2-amino-4-thiazolinone (**L₁**), namely its complexes with cobalt **[Co(L₁)₂Cl₂]** and silver **[Ag(L₁)₃NO₃]**, in ethanol. The spectrum of the free ligand exhibits two intense absorption bands with maxima at 220 nm (A = 2.3476) and 250 nm (A = 1.0257). These bands are due to the π → π* and n → π* electronic transitions within the conjugated system of the heterocyclic 2-amino-4-thiazolinone (**L₁**) ring.

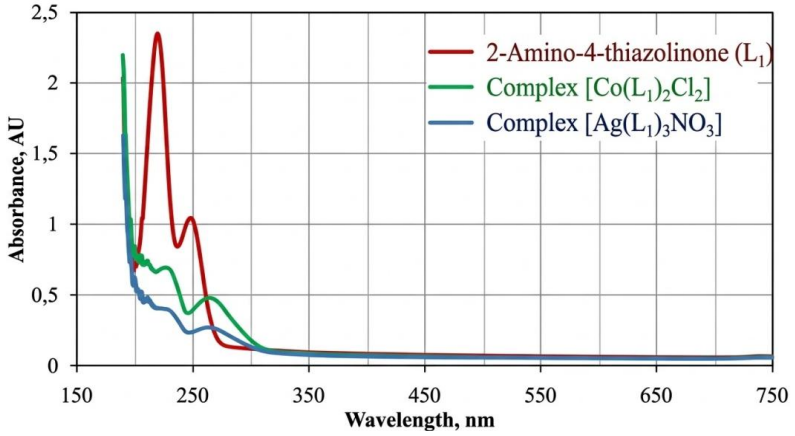


Figure 5. Electronic absorption spectra of free 2-amino-4-thiazolinone (**L₁**) and the corresponding cobalt (II) **[Co(L₁)₂Cl₂]** and silver (I) **[Ag(L₁)₃NO₃]** complexes in ethanol

The complexation process is accompanied by significant changes in the spectral profile [47]. For the cobalt complex **[Co(L₁)₂Cl₂]**, a bathochromic shift of the first band to 227.5 nm (Δλ = 7.5 nm) is observed. This indicates a decrease in the energy gap between the Highest Occupied Molecular Orbital (HOMO) and the Lowest Unoccupied Molecular Orbital (LUMO) of the ligand **L₁** upon coordination with the Co^{2+} ion. For the silver complex **[Ag(L₁)₃NO₃]**, a pronounced hypsochromic shift to 209 nm (Δλ = 11 nm) was recorded. This shift toward the shorter wavelength region indicates the involvement of the lone pair of the heteroatom (likely the ring nitrogen atom) in the coordination bond with the Ag^{+} ion, which leads to a disruption of the initial conjugation and an increase in the transition energy

The second absorption maximum of the ligand (250.5 nm) undergoes a bathochromic shift to 264 nm (Δλ = 13.5 nm) in both the cobalt and silver complexes. The identical position of this maximum for both the cobalt and silver compounds indicates a similar nature of electronic perturbations within the thiazoline moiety upon interaction with *d*-metals.

A characteristic feature of all recorded spectra is a sharp decrease in absorption intensity (hypochromic effect) from 2.35 to values ranging between 0.26–0.69. This effect may be a consequence of changes in the symmetry of the ligand molecule, the distortion of its planarity upon incorporation into the coordination polyhedron, or a change in the probability of electronic transitions due to partial ligand-to-metal charge transfer (LMCT).

Thus, the bathochromic and hypsochromic shifts of the main maxima, in conjunction with the hypochromic effect, unequivocally confirm the formation of metal–ligand chemical bonds and the synthesis of new coordination compounds.

Study of Antimicrobial Activity

Recently, 2-aminothiazoles have become essential heterocyclic compounds owing to their versatile applications in various fields. It also plays a major role in the pharmaceutical industry and is a critical scaffold for drug discovery [1–3]. Among heterocyclic compounds, thiazolidinone represents a wide range of biological activities including anticancer, antimicrobial, antidiabetic, and several others. The presence of N–C–S linkage along with carbonyl contributes to its therapeutic potential. Furthermore, the structure–activity relationship (SAR) and biological implications of various thiazolidinone derivatives are discussed, emphasizing their promising therapeutic leads for future drug discovery [1, 4, 6].

The investigation of antimicrobial properties represents a crucial step in assessing the biological relevance of transition metal complexes. In this work, the antibacterial and antifungal activities of 2-amino-4-thiazolone (**L₁**) and the obtained **[Co(L₁)₂Cl₂]** and **[Ag(L₁)₃NO₃]** complexes were evaluated using the agar well diffusion method and the microdilution broth assay. The comprehensive experimental data and comparative analysis with commercial reference drugs are presented in Table 2

Table 2

Antimicrobial activity (zone of inhibition, mm) and minimum inhibitory concentration (MIC, μg/mL) of 2-Amino-4-thiazolinone (L₁), complexes $[Co(L_1)_2Cl_2]$ **and** $[Ag(L_1)_3NO_3]$ **and reference drugs**

Compound	Zone of inhibition, mm					MIC, μg/mL
	S. aureus	*B. subtilis*	*E. coli*	*P. aeruginosa*	*C. albicans*	
2-Amino-4-thiazolinone (**L₁**)	12 ± 0.4	13 ± 0.5	11 ± 0.3	10 ± 0.4	12 ± 0.6	64–128
Complex [Co(L₁)₂Cl₂]	17 ± 0.5	18 ± 0.6	16 ± 0.4	15 ± 0.5	17 ± 0.4	16–32
Complex [Ag(L₁)₃NO₃]	24 ± 0.6	25 ± 0.7	23 ± 0.5	22 ± 0.6	26 ± 0.5	4–8
Ampicillin	28 ± 0.8	29 ± 0.7	–	–	–	2–4
Ciprofloxacin	–	–	30 ± 0.7	28 ± 0.8	–	0.25–0.5
Fluconazole	–	–	–	–	22 ± 0.6	0.5–1

Note – Values represent mean ± SD (n = 3). – indicates no activity or not tested

It is worth noting that the free heterocyclic ligand, 2-amino-4-thiazolone (**L₁**), displayed moderate inhibitory activity during preliminary screening, suggesting a limited capability to penetrate microbial cell barriers on its own. In stark contrast, its coordination to Co(II) and Ag(I) metal centers led to a remarkable synergistic enhancement of antimicrobial potency. This phenomenon complies with Tweedy's chelation theory [23, 48], suggesting that the reduction of the metal ion's polarity increases the lipophilicity of the entire molecular architecture, thereby facilitating its permeation through the lipid layer of microbial cell membranes.

To provide a visual correlation with the quantitative data detailed in Table 2 and discussed above, a series of representative photographic results from the agar well diffusion and disk diffusion assays are presented below (refer to Figure 6). These images vividly illustrate the zones of inhibition observed for 2-amino-4-thiazolinone ($\mathbf{L_1}$), its $\mathbf{[Co(L_1)_2Cl_2]}$ and $\mathbf{[Ag(L_1)_3NO_3]}$ complexes, and standard reference antibiotics against the five test microorganisms, validating the synergistic effect.

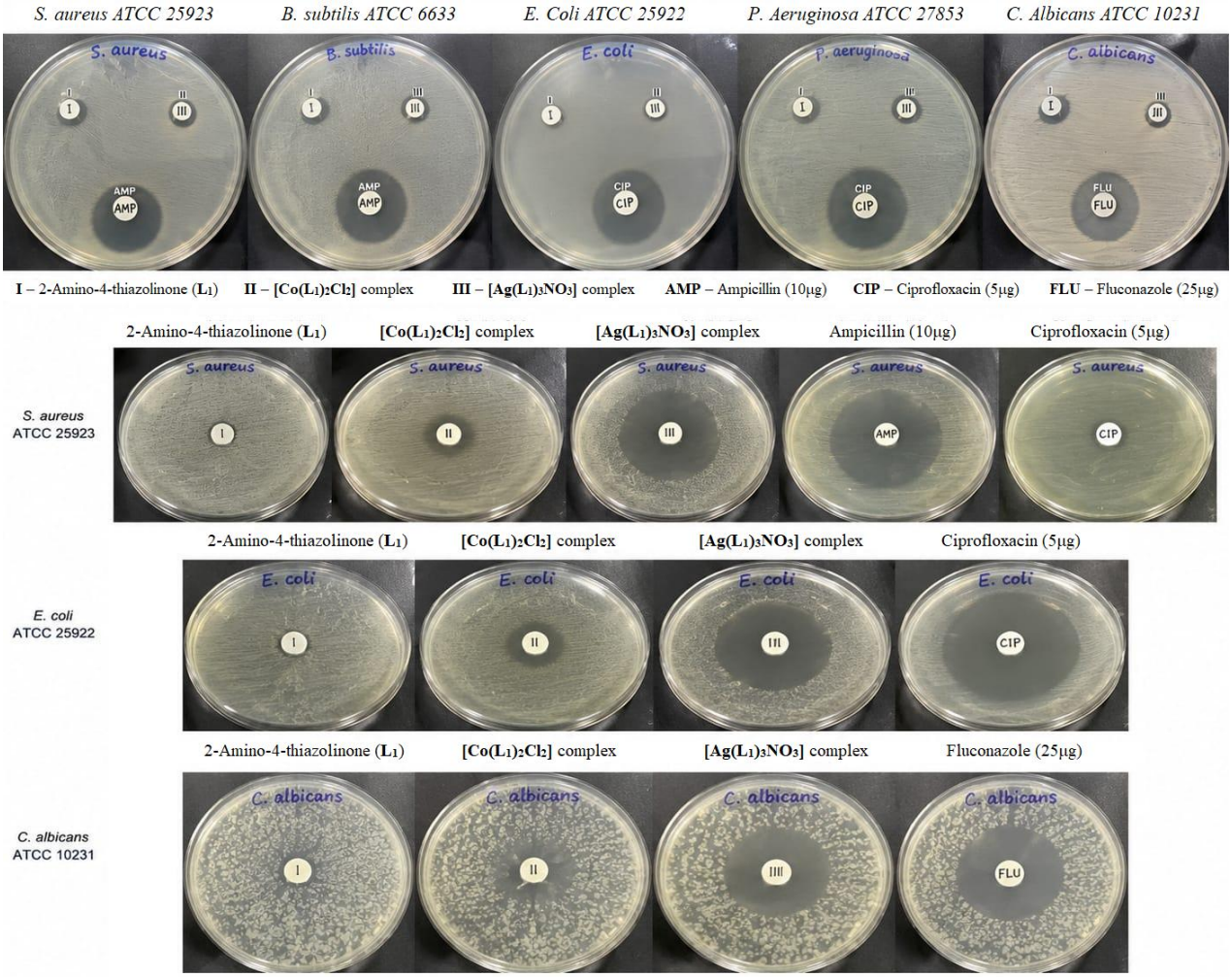


Figure 6. Representative images of the antimicrobial activity of 2-amino-4-thiazolinone ($\mathbf{L_1}$), its cobalt $\mathbf{[Co(L_1)_2Cl_2]}$ and silver $\mathbf{[Ag(L_1)_3NO_3]}$ complexes, and reference drugs (ampicillin, ciprofloxacin, and fluconazole) against the tested microbial strains, as determined by the agar well diffusion method.

The uncoordinated ligand 2-amino-4-thiazolinone ($\mathbf{L_1}$) demonstrated low antimicrobial activity against all tested microorganisms. The zones of inhibition against *S. aureus* and *B. subtilis* were 12 ± 0.4 and 13 ± 0.5 mm, respectively, which were notably lower than those observed for the reference drug ampicillin (28 ± 0.8 and 29 ± 0.7 mm). Against Gram-negative strains, $\mathbf{L_1}$ exhibited inhibition zones of 11 ± 0.3 mm (*E. coli*) and 10 ± 0.4 mm (*P. aeruginosa*), while antifungal activity against *C. albicans* was 12 ± 0.6 mm. The minimum inhibitory concentration (MIC) values ranged from 64 to 128 µg/mL. This moderate-low activity of $\mathbf{L_1}$ may be attributed to its limited capability to permeate through microbial cell barriers independently. Unlike the metal complexes, the uncoordinated ligand does not benefit from the reduction of polarity that occurs upon coordination with metal centers [23–25, 49].

Complex $\mathbf{[Co(L_1)_2Cl_2]}$ exhibited enhanced antimicrobial activity, surpassing free $\mathbf{L_1}$ across all tested strains. The zones of inhibition were 17 ± 0.5 mm against *S. aureus*, 18 ± 0.6 mm against *B. subtilis*, 16 ± 0.4 mm against *E. coli*, and 15 ± 0.5 mm against *P. aeruginosa*. Antifungal activity against *C. albicans* reached an inhibition zone of 17 ± 0.4 mm. The MIC values (16–32 µg/mL) were significantly lower than those of free ligand. The enhanced potency of the cobalt(II) complex relative to $\mathbf{L_1}$ can be explained by Overtone's concept and Tweedy's chelation theory: coordination to the Co(II) center reduces the polarity of the metal ion via partial sharing of its positive charge with donor atoms and electron delocalization over the chelate

ring. This lipophilic character facilitates penetration through the lipid bilayer of microbial cell membranes [23–25, 48–50]. Furthermore, Co(II) complexes are known to interfere with bacterial DNA transcription and critical enzymatic pathways, further contributing to their elevated antibacterial profile [51].

Complex [Ag(L_1)$_3$$NO_3$] displayed the most potent antimicrobial activity among all synthesized compounds, with inhibition zones of 24 ± 0.6 mm (*S. aureus*), 25 ± 0.7 mm (*B. subtilis*), 23 ± 0.5 mm (*E. coli*), 22 ± 0.6 mm (*P. aeruginosa*), and 26 ± 0.5 mm (*C. albicans*). The MIC values (4–8 μg/mL) were the lowest in the series, approaching or even matching the activity of the reference drugs for several strains. The superior antimicrobial performance of **[Ag(L_1)$_3$$NO_3$]** is attributed to a synergistic effect between the silver(I) ion and the aminothiazolone ligand. Silver(I) ions are well-established antimicrobial agents operating through multi-target mechanisms, including cell membrane disruption, inhibition of respiratory chain enzymes, ROS generation, and interference with DNA replication [50–52]. Coordination with ligand **L_1** amplifies these bioeffects by reducing complex polarity in accordance with Tweedy's chelation theory, thereby facilitating membrane penetration and improving cellular uptake [53-54]. Although silver coordination compounds often undergo ligand dissociation and slow Ag^+ release in aqueous culture media, the presence of the organic ligand scaffold modulates both drug solubility and ion delivery dynamics, allowing the complex to act as an effective delivery carrier. While formal silver-release kinetics were not quantitatively determined in this study, the combined mechanisms yield enhanced broad-spectrum activity against both bacterial and fungal pathogens, highlighting **[Ag(L_1)$_3$$NO_3$]** as a promising scaffold for novel antimicrobial drug design.

Taken together, these results demonstrate a clear structure–activity relationship (SAR) within the series: free 2-Amino-4-thiazolinone (**L_1**) < **Complex [Co(L_1)$_2$$Cl_2$]** < **Complex [Ag($L_1$)$_3$$NO_3$]**. Metal complexation significantly enhances antimicrobial potency relative to organic precursor, and nature of the metal ion is primary determinant of biological activity. These findings are consistent with previously reported coordination compounds based on heterocyclic ligands [55–57]. Furthermore, they support the rationale for the further development of silver(I)-based coordination complex architectures as promising candidates for antimicrobial applications. This is well aligned with established agents utilizing silver salts coupled with thiazole derivatives, which have proven effective as targeted antifungal remedies against *Candida tropicalis*, *Candida krusei*, and *Candida glabrata* strains [58].

Molecular Docking Studies Against Bacterial and Fungal Targets

To provide a rational structural context for the observed in vitro antimicrobial profile (Table 2), molecular docking was performed against five representative microbial targets: DNA gyrase (E. coli / P. aeruginosa, PDB ID: 6RKS; S. aureus, PDB ID: 2XCT), penicillin-binding proteins (E. coli, PDB ID: 2EXB; S. aureus, PDB ID: 1VQQ), and CYP51 (Candida albicans, PDB ID: 4WMZ). These specific crystallographic structures were selected because they represent co-crystallized complexes containing the exact same reference drugs – Ciprofloxacin, Ampicillin, and Fluconazole, respectively − that were employed as positive controls in the experimental bioassays. Docking into these validated binding pockets allowed comparison between the binding affinities (ΔG, Table 3) and binding modes of the free ligand **L_1**, its metal complexes, and the native reference inhibitors.

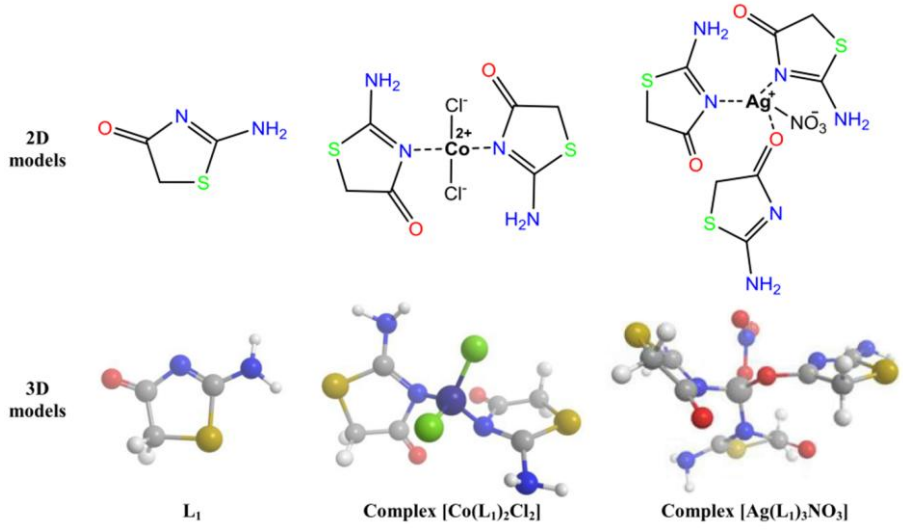


Figure 7. 2D and 3D molecular structures of 2-amino-4-thiazolinone (**L1**) and its cobalt(II) and silver(I) complexes

For the in silico assessment of the bioactive potential of 2-amino-4-thiazolinone **L_1** and its complexes **$[Co(L_1)_2Cl_2]$** and **$[Ag(L_1)_3NO_3]$**, the initial 2D molecular models derived from crystallographic data were transformed into 3D structures using Chem3D software, followed by geometry optimization employing the MMFF94 force field (Figure 7).

The optimized 3D geometries of **L_1**, its cobalt(II) and silver(I) complexes, and the reference standards (Figure 7) were subsequently converted into PDB format and subjected to ligand preparation protocols prior to docking in AutoDock Vina; the calculated binding affinities (kcal/mol) for each target protein are compiled in Table 3.

Table 3

Binding affinity values (ΔG, kcal/mol) of ligand L_1, its metal complexes, and reference drugs calculated via AutoDock Vina against target proteins (PDB IDs: 6RKS, 2XCT, 2EXB, 1VQQ, and 4WMZ)

Binding affinity, kcal/mol / *Compound*	6RKS	2XCT	2EXB	1VQQ	4WMZ
2-Amino-4-thiazolinone L_1	−4.6	−5.1	−3.9	−4.4	−4.6
Complex $[Co(L_1)_2Cl_2]$	−7.4	−7.5	−5.8	−6	−6.2
Complex $[Ag(L_1)_3NO_3]$	−7.4	−8.8	−7.2	−7.4	−7.2
Reference Drug					
Ciprofloxacin	−8.2	−9.2	−7.4	−7.9	−8.7
Ampicillin	−7.2	−9.4	−7.4	−7.2	−8.1
Fluconazole	−8.2	−8.7	−6.6	−6.6	−7.4

As can be seen in Table 3, the *in silico* docking results reveal a clear trend in binding affinities (ΔG) across all target proteins, mirroring the experimental SAR observations. The uncomplexed ligand **L_1** exhibited the weakest binding affinity across all receptors, with values ranging from −3.9 to −5.1 kcal/mol. Coordination with metal ions led to a pronounced enhancement in binding potency; the cobalt complex **$[Co(L_1)_2Cl_2]$** demonstrated improved affinities (−5.8 to −7.5 kcal/mol), while the silver complex **$[Ag(L_1)_3NO_3]$** displayed the strongest interactions among the synthesized compounds, reaching −8.8 kcal/mol against *S. aureus* DNA gyrase (2XCT) and −7.2 to −7.4 kcal/mol across the remaining targets. Notably, the binding energy of **$[Ag(L_1)_3NO_3]$** against *E. coli* penicillin-binding protein (2EXB, −7.2 kcal/mol) and *S. aureus* penicillin-binding protein (1VQQ, −7.4 kcal/mol) was nearly equipotent to the reference antibiotic Ampicillin (−7.4 and −7.2 kcal/mol, respectively), reinforcing the pivotal role of the silver core in maximizing target site interactions. Taken together, these *in silico* results demonstrate a clear structure–activity relationship within the series: free 2-amino-4-thiazolinone (**L_1**) < **Complex $[Co(L_1)_2Cl_2]$** < **Complex $[Ag(L_1)_3NO_3]$**, which is in full agreement with the experimental findings described in the previous section.

To elucidate the specific binding modes and molecular forces driving these affinities, the key intermolecular interactions between the studied compounds and target proteins, including hydrogen bonding, hydrophobic, electrostatic, and steric contact points, were analyzed (Table S1) and visualized (Figure S11). Since docking simulations demonstrated the strongest binding interactions with the *S. aureus* DNA gyrase target (PDB ID: 2XCT), the key ligand–amino acid contact maps for this protein are highlighted in Table 4 and Figure 8, with the full interaction profile for all other complexes detailed in Supplementary Materials.

Table 4

Intermolecular interactions formed by ligand L_1, complexes $[Co(L_1)_2Cl_2]$ and $Ag(L_1)_3NO_3]$, and reference drugs with 2XCT target protein (*Staphylococcus aureus* + Ciprofloxacin)

Compound	Conventional Hydrogen Bond	π-Alkyl	Carbon Hydrogen Bond	Halogen
2-Amino-4-thiazolinone **L_1**	THR1181	–	–	–
Complex $[Co(L_1)_2Cl_2]$	SER1330, ASN1182	–	–	–
Complex $[Ag(L_1)_3NO_3]$	THR1329	–	–	–
Ciprofloxacin	–	–	–	–
Ampicillin	GLY1332	PHE1331, VAL1268, PRO1326	PHE1331, SER1330	PHE1266, GLN1267
Fluconazole	SER1173	–	–	–

Detailed analysis of the specific ligand–receptor interactions in Tables 4 and Table S1 clarifies the structural origin of the enhanced binding affinities observed for the metal complexes. Free ligand $\mathbf{L_1}$ exhibits primarily conventional hydrogen bonds and localized hydrophobic contacts across the active sites, though in some instances (e.g., against 2EXB and 1VQQ), its binding is accompanied by unfavorable donor–donor or electrostatic contacts, which accounts for its lower binding affinity. Coordination into the cobalt complex $\mathbf{[Co(L_1)_2Cl_2]}$ eliminates these unfavorable interactions and forms stabilized hydrogen-bonding networks with key catalytic residues (e.g., SER1330/ASN1182 in 2XCT and SER420/SER62/ASN308 in 2EXB). Crucially, the silver complex $\mathbf{[Ag(L_1)_3NO_3]}$ displays the highest density and diversity of stabilizing non-covalent forces: it establishes extensive multi-point conventional hydrogen bonds (notably via TYR149, GLU153, ASN148, LYS64, and TYR63 in 6RKS; ILE471, CYS470, TYR140, HIS468, and ARG385 in 4WMZ) complemented by favorable electrostatic forces (attractive charge interactions with ARG65, ASP139, ASP304, HIS129, GLU61 in 1VQQ; ASP150 in 6RKS) and hydrophobic π-alkyl/π-anion interactions. These extensive interactions with active-site residues match or exceed those of the reference drugs Ciprofloxacin, Ampicillin, and Fluconazole. This explains the higher antimicrobial potency and stability of the silver complex.

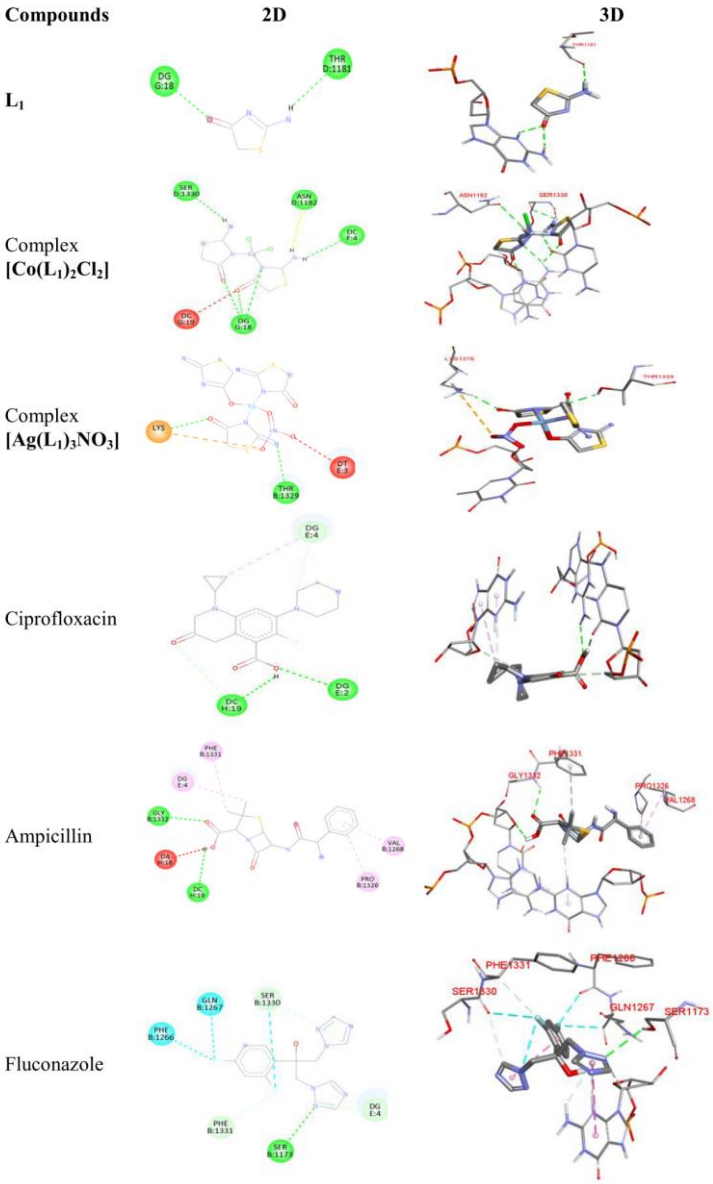


Figure 8. 2D and 3D visualizations of key active-site amino acid interactions with ligands for the *Staphylococcus aureus* DNA gyrase target protein (PDB ID: 2XCT)

Overall, the in silico molecular docking findings correlates with the experimental SAR data and provide a atomistic rationale for the experimentally observed bioactivity of the synthesized compounds. The enhanced binding affinity of the silver complex stems from its tris-ligand coordination, which creates an expanded, highly complementary three-dimensional architecture capable of forming a denser network of non-covalent interactions within the active site. These results not only confirm the strategic advantage of metal complexation in enhancing antimicrobial efficacy, but also highlight the silver(I) complex as a highly promising lead candidate for further development of antimicrobial agents.

Conclusions

In summary, this work presents a comprehensive investigation into the pH-controlled synthesis, structural characterization, and preliminary biological evaluation of novel cobalt(II) and silver(I) complexes based on 2-amino-4-thiazolinone (**L_1**).

Fine-tuning the pH during the neutralization of 2-amino-4-thiazolinone hydrochloride (**L_1H**) allowed for the selective isolation of the amino (**L_1**, pH = 11) and imino (**L_2**, pH = 6.5) tautomeric forms. Their structural integrity and tautomeric behavior in solution were unambiguously established using ^{1}H and ^{13}C NMR spectroscopy.

Complexation of **L_1H** with cobalt(II) chloride and silver(I) nitrate afforded **$[Co(L_1)_2Cl_2]$** and **$[Ag(L_1)_3NO_3]$** coordination architectures, respectively. X-ray diffraction (XRD), alongside IR and UV-Vis spectroscopic analyses, demonstrated that, **$[Co(L_1)_2Cl_2]$** and crystallizes in the triclinic P1 space group, adopting a distorted tetrahedral geometry around the Co(II) center via monodentate coordination of the endocyclic ring nitrogen atoms of two **L_1**ligands. And **$[Ag(L_1)_3NO_3]$** crystallizes in the monoclinic P21/n space group, featuring an irregular coordination polyhedron formed by two endocyclic nitrogen atoms, a exocyclic carbonyl oxygen atom from a neighboring ligand, and a weakly bound nitrate anion, resulting in self-assembled chains.

In vitro biological testing against Gram-positive (*S. aureus*, *B. subtilis*) and Gram-negative (*E. coli*, *P. aeruginosa*) bacteria, as well as the fungal strain *C. albicans*, established a clear structure–activity relationship (SAR) in the order: 2-amino-4-thiazolinone (**L_1**) < **Complex $[Co(L_1)_2Cl_2]$** < **Complex $[Ag(L_1)_3NO_3]$**. While the uncoordinated ligand **L_1** exhibited low-to-moderate antimicrobial effects (MIC = 64–128 μg/mL), metal coordination significantly enhanced the biological efficiency. The silver(I) complex **$[Ag(L_1)_3NO_3]$** displayed remarkable broad-spectrum antibacterial and antifungal potency (MIC = 4–8 μg/mL), approaching the effectiveness of reference therapeutic agents (Ampicillin, Ciprofloxacin, and Fluconazole). This enhancement aligns with Tweedy's chelation theory and the intrinsic bactericidal activity of the Ag^{+} center.

Molecular docking studies against therapeutic target enzymes (DNA gyrase, penicillin-binding proteins, and CYP51) strongly correlated with the experimental SAR results. Complex **$[Ag(L_1)_3NO_3]$** exhibited the highest binding affinity (up to -8.8 kcal/mol against *S. aureus* DNA gyrase), stabilizing within the active pockets through strong hydrogen bonding, ionic, and hydrophobic interaction networks.

Overall, these findings demonstrate the efficacy of transitioning from heterocyclic organic ligands to coordination complexes, identifying **$[Ag(L_1)_3NO_3]$** as a promising lead candidate for the further development of novel antibacterial and antifungal therapeutics.

Supporting Information

The Supporting Information is available free at https://ejc.buketov.edu.kz/ejc/article/view/822/447

*Author Information**

**The authors' names are presented in the following order: First Name, Middle Name and Last Name*

Aigul Amanbekovna Zhortarova – PhD student, Department of Organic Chemistry and Polymers, Buketov Karaganda National Research University, Universitetskaya str., 28, 100024, Karaganda, Kazakhstan; e-mail: aygul.zhortarova.90@mail.ru; https://orcid.org/0000-0001-9307-2342

Vojtěch Kubíček – Doc. RNDr., PhD, Department of Inorganic Chemistry, Faculty of Science, Charles University, Hlavova 2030, 128 43 Prague 2, Prague, Czech Republic; e-mail: kubicek@natur.cuni.cz; https://orcid.org/0000-0003-0171-5713

Marat Kirimbayevich Ibrayev – Doctor of Chemical Sciences, Research Professor, Department of Organic Chemistry and Polymers, Buketov Karaganda National Research University, Universitetskaya street, 28, 100024, Karaganda, Kazakhstan; e-mail: mkibr@mail.ru; https://orcid.org/0000-0003-0798-5562

Svetlana Yur'evna Panshina *(corresponding author)* – Candidate of Chemical Sciences, Assistant Professor, Department of Organic Chemistry and Polymers, Buketov Karaganda National Research University, Universitetskaya street, 28, 100024, Karaganda, Kazakhstan; e-mail: janim_svetatusik@mail.ru; https://orcid.org/0000-0001-6824-2645

Irina Anatolievna Pustolaikina – Candidate of Chemical Sciences, Associate Professor, Department of Physical and Analytical Chemistry, Buketov Karaganda National Research University, Universitetskaya street, 28, 100024, Karaganda, Kazakhstan; e-mail: ipustolaikina@gmail.com; https://orcid.org/0000-0001-6319-666X

Roza Battalovna Seidakhmetova – Candidate of Medical Sciences, Professor, Karaganda Medical University, Gogol Street, 40, 100000, Karaganda, Kazakhstan; e-mail: roza77124@gmail.com; https://orcid.org/0000-0002-1990-4961

Author Contributions

The manuscript was written through contributions of all authors. All authors have given approval to the final version of the manuscript. CRediT: **Aigul A. Zhortarova** – Conceptualization, Data Curation, Investigation, Methodology, Supervision, Visualization, Writing – Original Draft, Writing – Review & Editing. **Vojtěch Kubíček** – Conceptualization, Data Curation, Methodology, Project Administration, Supervision, *Resources,* Writing – Original Draft, Writing – Review & Editing. **Marat K. Ibrayev** – Conceptualization, Methodology, Project Administration, Supervision, *Resources.* **Svetlana Y. Panshina** – Conceptualization, Data Curation, Methodology, Supervision, Visualization, Writing – Review & Editing, Software. **Irina A. Pustolaikina** – Formal Analysis, Methodology, Investigation, Software, Visualization, Validation. **Roza B. Seidakhmetova** - Formal Analysis, Methodology, Investigation, Validation, Software, Visualization

Acknowledgments

We thank Charles University for financial support to our research groups.

Conflicts of Interest

The authors declare no conflict of interest.

References

1 Bhatia, R. (2026). Thiazolidinone spirocycles: synthetic routes and biological implications. *Journal of Heterocyclic Chemistry*, *63*, 818–852 https://doi.org/10.1002/jhet.70175

2 Upadhyaya, A., & Dwivedi, J. (2026). Recent advances in the synthesis of biologically and pharmaceutically active thiazole and its analogues. *Journal of Heterocyclic Chemistry*, *63*, 748–772. https://doi.org/10.1002/jhet.70170

3 Migulin, A. V., Milyutin, C. V., & Komogortsev, A. N. (2025). Design, Synthesis, and Biological Evaluation of Some New Thiazole-Based Compounds as Antioxidant and Antimicrobial Agents. *Journal of Heterocyclic Chemistry*, *63*, 567–578. https://doi.org/10.1002/jhet.70155

4 Shehab, W. S., Abdelaziz, M., Elhoseni, N. K. R., Assy, M. G., Abdellattif, M. H., & Hamed, E. O. (2022). Design, synthesis, molecular docking, and evaluation of antioxidant and antimicrobial activities for novel 3-phenylimidazolidin-4-one and 2-aminothiazol-4-one derivatives. *Molecules*, *27*(3), 767. https://doi.org/10.3390/molecules27030767

5 Kupczyk, D., Studzińska, R., Bilski, R., Baumgart, S., Kołodziejska, R., & Woźniak, A. (2020). Synthesis of novel 2-(isopropylamino)thiazol-4(5H)-one derivatives and their inhibitory activity of 11β-HSD1 and 11β-HSD2 in aspect of carcinogenesis prevention. *Molecules*, *25*(18), 4233. https://doi.org/10.3390/molecules25184233

6 Zhortarova, A. A., Kubíček, V., Ibrayev, M. K., Panshina, S. Yu., & Kurmanova, A. F. (2026). Synthesis and structural features of novel phosphorylated aminothiazole. *Tetrahedron*, 200, 135426. https://doi.org/10.1016/j.tet.2026.135426

7 Khalifa, M. E. (2018). Recent developments and biological activities of 2-aminothiazole derivatives. *Acta Chimica Slovenica*, *65*(1), 1–22. https://doi.org/10.17344/acsi.2017.3547

8 Patt, W. C., Hamilton, H. W., Taylor, M. D., Ryan, M. J., Taylor, D. G., Jr., Connolly, C. J. C., Doherty, A. M., Klutchko, S. R., Sircar, I., & Steinbaugh, B. A. (1992). Structure–activity relationships of a series of 2-amino-4-thiazole-containing renin inhibitors. *Journal of Medicinal Chemistry*, *35*(14), 2562–2572. https://doi.org/10.1021/jm00092a006

9 Ramsh, S. M., Smorygo, N. A., & Ginak, A. I. (1984). Structure of 2-amino-4-thiazolinone. *Chemistry of Heterocyclic Compounds*, *20*(8), 865–869. https://doi.org/10.1007/BF00513571

10 Ramsh, S. M., Smorygo, N. A., & Khrabrova, E. S. (1985). Structure of 2-amino-4-thiazolinone and its 2-aryl derivatives in the crystalline state. *Chemistry of Heterocyclic Compounds*, *21*, 24–29. https://doi.org/10.1007/BF00505893

11 Raper, E. S., Oughtred, R. E., Nowell, I. W., & March, L. A. (1981). The structure of bis(2-aminothiazole)dichlorocobalt(II). *Acta Crystallographica Section B*, 37, 928–930. https://doi.org/10.1107/S0567740881004639

12 Bahsis, L., Hrimla, M., Ben El Ayouchia, H., Anane, H., Julve, M., & Stiriba, S. E. (2020). 2-Aminobenzothiazole-containing copper(II) complex as catalyst in click chemistry: an experimental and theoretical study. *Catalysts*, 10, 776. https://doi.org/10.3390/catal10070776

13 Keri, R. S., Patil, M. R., Patil, S. A., & Budagumpi, S. (2015). A comprehensive review in current developments of benzothiazole-based molecules in medicinal chemistry. *European Journal of Medicinal Chemistry*, 89, 207–251. https://doi.org/10.1016/j.ejmech.2014.10.059

14 Drzał, W., & Trotsko, N. (2025). Review of recent advances in thiazolidin-4-one derivatives as promising antitubercular agents (2021–present). *Molecules*, 30, 2201. https://doi.org/10.3390/molecules30102201

15 Juhás, M., Bachtíková, A., Nawrot, D. E., Hatoková, P., Pallabothula, V. S. K., Diepoltová, A., Janďourek, O., Bárta, P., Konečná, K., Paterová, P., Šesták, V., & Zitko, J. (2022). Improving Antimicrobial Activity and Physico-Chemical Properties by Isosteric Replacement of 2-Aminothiazole with 2-Aminooxazole. *Pharmaceuticals*, 15, 580. https://doi.org/10.3390/ph15050580

16 Loukrakpam, D. C., Mishra, D., Begum, J., & Phukan, P. (2023). TsNBr2 promoted cascade formation of C–N and C–S bond: Metal-free synthesis of 2-aminothiazoles from ketones or ketoximes using thiourea. *Tetrahedron*, 149, 133721. https://doi.org/10.1016/j.tet.2023.133721

17 Zhang, Q., Wu, J., Pan, Z., Zhang, W., & Zhou, W. (2021). A one-pot synthesis of 2-aminothiazoles via the coupling of ketones and thiourea using I2/dimethyl sulfoxide as a catalytic oxidative system. *Journal of Chemical Research*, 45(1–2), 89–94. https://doi.org/10.1177/1747519820930

18 Kalhor, M., Vahedi, Z., & Gharoubi, H. (2023). Design of a new method for one-pot synthesis of 2-amino thiazoles using trichloroisocyanuric acid in the presence of a novel multi-functional and magnetically catalytic nanosystem: Ca/4-MePy-IL@ZY-Fe3O4. *RSC Advances*, 13(13), 9208–9221. https://doi.org/10.1039/d3ra00758h

19 Fekri, R., Salehi, M., Asadi, A., & Kubicki, M. (2019). Synthesis, characterization, anticancer and antibacterial evaluation of Schiff base ligands derived from hydrazone and their transition metal complexes. *Inorganica Chimica Acta*, 484, 245–254. https://doi.org/10.1016/j.ica.2018.09.022

20 Kayed, S. F., & Farina, Y. (2025). Synthesis, characterization and biological study of 2-acetylbenzothiophene 4-cyclohexyl-3-thiosemicarbazone ligand and its transition metal complexes. *Chemical Papers*, 79, 961–981. https://doi.org/10.1007/s11696-024-03829-0

21 Al-Qadsy, I., Saeed, W. S., Al-Owais, A. A., Semlali, A., Alrabie, A., Al-Faqeeh, L. A. S., ALSaeedy, M., Al-Adhreai, A., Al-Odayni, A. B., & Farooqui, M. (2023). Antimicrobial activity of novel Ni(II) and Zn(II) complexes with (E)-2-((5-bromothiazol-2-yl)imino)methyl)phenol ligand: synthesis, characterization and molecular docking studies. *Antibiotics*, 12(11), 1634. https://doi.org/10.3390/antibiotics12111634

22 Marlin Risana, M., Balasubramaniyan, S., Govindharaju, R., Mohamed Azharudeen, A., Mary Juliet, B., MukilMeenakshi, V., Alsaiari, A. A., Roy, A., Verma, R., & Sharma, K. (2024). Comprehensive investigation on fabrication, spectral characterization and biological importance of Co(II) and Ni(II) heteroleptic complexes. *Inorganica Chimica Acta*, 569, 122125. https://doi.org/10.1016/j.ica.2024.122125

23 Hassoon, A. A., Abulkhair, H. S., Ashour, R. H., Abdelsamea, M. M., Abdullah, H. O., Eldesoky, M. A., Shaban, A. R., John, P., & Ghaith, E. A. (2026). Rational design and synthesis of Co(II), Ni(II) and Cu(II) complexes bearing 1,2,4-triazole scaffold for biological applications. *RSC Advances*, 16, 14509–14524. https://doi.org/10.1039/d5ra09383j

24 Ebrahimipour, S. Y., Mohamadi, M., Castro, J., Mollania, N., Rudbari, H. A., & Saccá, A. (2015). Syntheses, characterizations, crystal structures, and biological activities of two new mixed ligand Ni(II) and Cu(II) Schiff base complexes. *Journal of Coordination Chemistry*, 68(4), 632–649. https://doi.org/10.1080/00958972.2014.1000883

25 Hussain, R., Rubab, S. L., Maryam, A., Ashraf, T., Arshad, M., Lal, K., Sumrra, S. H., Ashraf, S., & Ali, B. (2023). Synthesis, spectroscopic and nonlinear optical properties, and antimicrobial activity of Cu(II), Co(II), and Ni(II) complexes: experimental and theoretical studies. *ACS Omega*, 8(45), 42598–42609. https://doi.org/10.1021/acsomega.3c05322

26 26. Pearson, R. G. (1963). Hard and soft acids and bases. *Journal of the American Chemical Society*, 85(22), 3533–3539. https://doi.org/10.1021/ja00905a001

27 Pearson, R. G. (1968). Hard and soft acids and bases, HSAB, part I: fundamental principles. *Journal of Chemical Education*, 45(9), 581–587. https://doi.org/10.1021/ed045p581

28 Cotton, F. A., Wilkinson, G., Murillo, C. A., & Bochmann, M. (1999). *Advanced Inorganic Chemistry* (6th ed.). Wiley-Interscience.

29 Greenwood, N. N., & Earnshaw, A. (1997). *Chemistry of the Elements* (2nd ed.). Butterworth-Heinemann.

30 Kumar, A., Kumar, S., Jain, S., Kumar, P., & Goyal, R. (2013). Study of binding of pyridoacridine alkaloids on topoisomerase II using in silico tools. *Medicinal Chemistry Research*, 22(11), 5431–5441. https://doi.org/10.1007/s00044-013-0496-5

31 Clinical and Laboratory Standards Institute. (2018). *Performance Standards for Antimicrobial Disk Susceptibility Tests* (CLSI Standard M02, 13th ed.). Clinical and Laboratory Standards Institute, Wayne

32 Clinical and Laboratory Standards Institute. (2018). *Methods for Dilution Antimicrobial Susceptibility Tests for Bacteria That Grow Aerobically* (CLSI Standard M07, 11th ed.). Clinical and Laboratory Standards Institute, Wayne

33 Kukushkin, A. A., Kudashova, E. V., Root, E. V., Kositsyna, A. S., Ponomarev, I. S., Lyubyashkin, A. V., & Pustolaikina, I. A. (2025). Synthesis, Characterization and Computational Study of Novel Copper(II) Chelate Complexes Ligated by Pyridyl-Containing Beta-Diketonates. Eurasian Journal of Chemistry, 30(2(118)), 4–18. https://doi.org/10.31489/2959-0663/2-25-5

34 Trott, O., & Olson, A. J. (2010). AutoDock Vina: improving the speed and accuracy of docking with a new scoring function, efficient optimization, and multithreading. *Journal of Computational Chemistry*, 31(2), 455–461. https://doi.org/10.1002/jcc.21334

35 Stalinskaya, A. L., Pustolaikina, I. A., Kurmanova, A. F., Rakhimzhanova, A. S., Muzaparov, R. A., Normatov, S., Novikov, A. S., & Kulakov, I. V. (2025). Synthesis, characterization, and computational study of s-methylthio- and n-methylamine substituted epoxybenzo[7,8]oxocyno[4,3-b]pyridine derivatives. Journal of Molecular Structure, 1348, 143346. https://doi.org/10.1016/j.molstruc.2025.143346

36 Gaussian 16, Revision A.03, M. J. Frisch, G. W. Trucks, H. B. Schlegel, G. E. Scuseria, M. A. Robb, J. R. Cheeseman, G. Scalmani, V. Barone, G. A. Petersson, H. Nakatsuji, X. Li, M. Caricato, A. V. Marenich, J. Bloino, B. G. Janesko, R. Gomperts, B. Mennucci, H. P. Hratchian, J. V. Ortiz, A. F. Izmaylov, J. L. Sonnenberg, D. Williams-Young, F. Ding, F. Lipparini, F. Egidi, J. Goings, B. Peng, A. Petrone, T. Henderson, D. Ranasinghe, V. G. Zakrzewski, J. Gao, N. Rega, G. Zheng, W. Liang, M. Hada, M. Ehara, K. Toyota, R. Fukuda, J. Hasegawa, M. Ishida, T. Nakajima, Y. Honda, O. Kitao, H. Nakai, T. Vreven, K. Throssell, J. A. Montgomery, Jr., J. E. Peralta, F. Ogliaro, M. J. Bearpark, J. J. Heyd, E. N. Brothers, K. N. Kudin, V. N. Staroverov, T. A. Keith, R. Kobayashi, J. Normand, K. Raghavachari, A. P. Rendell, J. C. Burant, S. S. Iyengar, J. Tomasi, M. Cossi, J. M. Millam, M. Klene, C. Adamo, R. Cammi, J. W. Ochterski, R. L. Martin, K. Morokuma, O. Farkas, J. B. Foresman, and D. J. Fox, Gaussian, Inc., Wallingford CT, 2016.

37 Vanden Broeck, A., Lotz, C., Ortiz, J., & Lamour, V. (2019). Cryo-EM structure of the complete *E. coli* DNA gyrase nucleoprotein complex. *Nature Communications*, 10, 4935. https://doi.org/10.1038/s41467-019-12914-y

38 Bax, B. D., Chan, P. F., Eggleston, D. S., Fosberry, A., Gentry, D. R., Gorrec, F., Giordano, I., Hann, M. M., Hennessy, A., Hibbs, M., Huang, J., Jones, E., Jones, J., Brown, K. K., Lewis, C. J., May, E. W., Saunders, M. R., Singh, O., Spitzfaden, C. E., Shen, C., Shillings, A., Theobald, A. J., Wohlkonig, A., Pearson, N. D., & Gwynn, M. N. (2010). Type IIA topoisomerase inhibition by a new class of antibacterial agents. *Nature*, 466(7309), 935–940. https://doi.org/10.1038/nature09197

39 Kishida, H., Unzai, S., Roper, D. I., Lloyd, A., Park, S. Y., & Tame, J. R. H. (2006). Crystal structure of penicillin binding protein 4 (dacB) from *Escherichia coli*, both in the native form and covalently linked to various antibiotics. *Biochemistry*, 45(3), 783–792. https://doi.org/10.1021/bi051533t

40 Sagatova, A. A., Keniya, M. V., Wilson, R. K., Monk, B. C., & Tyndall, J. D. A. (2015). Structural insights into binding of the antifungal drug fluconazole to *Saccharomyces cerevisiae* lanosterol 14α-demethylase. *Antimicrobial Agents and Chemotherapy*, 59(8), 4982–4989. https://doi.org/10.1128/AAC.00925-15

41 Meng, X. Y., Zhang, H. X., Mezei, M., & Cui, M. (2011). Molecular docking: a powerful approach for structure-based drug discovery. *Current Computer-Aided Drug Design*, 7(2), 146–157. https://doi.org/10.2174/157340911795677602

42 Morris, G. M., Goodsell, D. S., Halliday, R. S., Huey, R., Hart, W. E., Belew, R. K., & Olson, A. J. (1998). Automated docking using a Lamarckian genetic algorithm and an empirical binding free energy function. *Journal of Computational Chemistry*, 19(14), 1639–1662. https://doi.org/10.1002/(SICI)1096-987X(19981115)19:14<1639::AID-JCC10>3.0.CO;2-B

43 da Silva Santos, J., Junior, J. J., & da Silva, F. M. (2018). 1,3-Thiazolidin-4-ones: biological potential, history, synthetic development and green methodologies. *Current Organic Synthesis*, 15(8), 1109–1123. https://doi.org/10.2174/1570179415666180919125625

44 Abdu-Allah, H. H. M., Abdel-Moty, S. G., El-Awady, R., & El-Shorbagi, A. N. A. (2016). Design and synthesis of novel 5-aminosalicylate (5-ASA)–4-thiazolinone hybrid derivatives with promising antiproliferative activity. *Bioorganic & Medicinal Chemistry Letters*, 26(7), 1647–1650. https://doi.org/10.1016/j.bmcl.2016.02.073

45 Steel, P. J., & Guard, J. A. M. (1994). Heterocyclic tautomerism. VI. A redetermination and reassignment of the structure of 2-aminothiazol-4(5H)-one (pseudothiohydantoin). *Acta Crystallographica Section C*, 50, 1721–1723. https://doi.org/10.1107/S0108270194004750

46 Smokal, V., Derkowska, B., Czaplicki, R., Krupka, O., Kolendo, A., & Sahraoui, B. (2009). Nonlinear optical properties of thiazolidinone derivatives. *Optical Materials*, 31(3), 554–557. https://doi.org/10.1016/j.optmat.2007.10.019

47 AbdelLatif, S. A., & Issa, Y. M. (2010). Spectroscopic, thermal and magnetic properties of some transition metal complexes derived from 1-phenyl-3-substituted-4-nitroso-5-pyrazolones. *Natural Science*, 2(9), 1035–1043. https://doi.org/10.4236/ns.2010.29127

48 Tweedy, B. G. (1964). Plant extracts with metal ions as potential antimicrobial agents. *Phytopathology*, 55, 910–914.

49 Noreen, S., & Sumrra, S. H. (2021). Aminothiazole-linked metal chelates: synthesis, density functional theory, and antimicrobial studies with antioxidant correlations. *ACS Omega*, 6(48), 33085–33099. https://doi.org/10.1021/acsomega.1c05290

50 Wozniczka, M., Lichawska, M., Sutradhar, M., Chmiela, M., Gonciarz, W., & Pajak, M. (2021). Chemical characterization and biological evaluation of new cobalt(II) complexes with bioactive ligands, 2-picolinehydroxamic acid and reduced Schiff base N-(2-hydroxybenzyl)alanine, in terms of DNA binding and antimicrobial activity. *Pharmaceuticals*, 14(12), 1254. https://doi.org/10.3390/ph14121254

51 Salleh, A., Naomi, R., Utami, N. D., Mohammad, A. W., Mahmoudi, E., Mustafa, N., & Fauzi, M. B. (2020). The potential of silver nanoparticles for antiviral and antibacterial applications: a mechanism of action. *Nanomaterials*, 10(8), 1566. https://doi.org/10.3390/nano10081566

52 More, P. R., Pandit, S., De Filippis, A., Franci, G., Mijakovic, I., & Galdiero, M. (2023). Silver nanoparticles: bactericidal and mechanistic approach against drug resistant pathogens. *Microorganisms*, 11(2), 369. https://doi.org/10.3390/microorganisms11020369

53 Varna, D., Geromichalou, E., Papachristou, E., Papi, R., Hatzidimitriou, A. G., Panteris, E., Psomas, G., Geromichalos, G. D., Aslanidis, P., Choli-Papadopoulou, T., & Angaridis, P. A. (2022). Biocompatible silver(I) complexes with heterocyclic thioamide ligands for selective killing of cancer cells and high antimicrobial activity – a combined in vitro and in silico study. *Journal of Inorganic Biochemistry*, 228, 111695. https://doi.org/10.1016/j.jinorgbio.2021.111695

54 Bensalah, D., Gurbuz, N., Özdemir, I., Gatri, R., Mansour, L., & Hamdi, N. (2023). Synthesis, characterization, antimicrobial properties, and antioxidant activities of silver-N-heterocyclic carbene complexes. *Bioinorganic Chemistry and Applications*, 2023(1), 3066299. https://doi.org/10.1155/2023/3066299

55 Sharma, B., Shukla, S., Rattan, R., Fatima, M., Goel, M., Bhat, M., Dutta, S., Ranjan, R. K., & Sharma, M. (2022). Antimicrobial agents based on metal complexes: present situation and future prospects. *International Journal of Biomaterials*, 2022(1), 6819080. https://doi.org/10.1155/2022/6819080

56 Andrejević, T. P., Aleksic, I., Kljun, J., Počkaj, M., Zlatar, M., Vojnovic, S., Nikodinovic-Runic, J., Turel, I., Djuran, M. I., & Glišić, B. Đ. (2023). Copper(ii) and silver(i) complexes with dimethyl 6-(pyrazine-2-yl)pyridine-3,4-dicarboxylate (py-2pz): the influence of the metal ion on the antimicrobial potential of the complex. *RSC Advances*, 13(7), 4376–4393. https://doi.org/10.1039/d2ra07401j

57 Ran, K., Gao, C., Deng, H., Lei, Q., You, X., Wang, N., Shi, Y., Liu, Z., Wei, W., Peng, C., Xiong, L., Xiao, K., & Yu, L. (2016). Identification of novel 2-aminothiazole conjugated nitrofuran as antitubercular and antibacterial agents. *Bioorganic & Medicinal Chemistry Letters*, 26(15), 3669–3674. https://doi.org/10.1016/j.bmcl.2016.05.088

58 Gein, V. L., Bobrovskaya, O. V., Russkikh, A. A., Novikova, V. V., & Makhmudov, R. R. (2021). *Use of silver salt of N-{4-[(1,3-thiazol-2-yl)sulfamoyl]phenyl}-1-phenyl-5-(4-ethoxyphenyl)pyrazole-3-carboxamide as an antifungal agent against strains of fungi C. tropicalis, C. krusei and C. glabrata* (Russian Patent No. RU 2763724 C1). Federal Service for Intellectual Property. https://patents.google.com/patent/RU2763724C1/ru